ON THE ROLE OF AIR-SEA-ICE INTERACTIONS OFF EAST ANTARCTICA

A Thesis

by

CODY JAMES WEBB

Submitted to the Office of Graduate and Professional Studies of
Texas A&M University
in partial fulfillment of the requirements for the degree of

MASTER OF SCIENCE

Chair of Committee,	Alejandro H. Orsi
Committee Members,	Achim Stoessel
	John Nielsen-Gammon
Head of Department,	Shari Yvon-Lewis

December 2017

Major Subject: Oceanography

ABSTRACT

In some segments of the Antarctic continental shelf, salt released during sea-ice production transforms near-freezing Antarctic surface waters into saltier (S > 34.52) and denser Shelf Water. Near the shelf break of these locations, somewhat attenuated Shelf Water outflows and sinks down the continental slope, entraining relatively warmer Circumpolar Deep Water to form Antarctic Bottom Water. Thus, sea-ice formation plays a climate-relevant role in the global Meridional Overturning Circulation.

Similar geographic and oceanographic characteristics are found off the Sabrina and Adélie coasts in East Antarctica, therefore Shelf Water is unexpectedly found only in the Adélie Depression and lacking in the Sabrina Basin. A combination of in-situ, remote, and reanalysis datasets from 2003-2015 are used in this study to investigate the conditions leading to Sabrina's relatively passive role. For the first time, sea-ice production rates are estimated combining both the net sea-ice volume exchanged across the shelf break (export) and the volume variability farther inshore (growth).

The Sabrina Basin produces an average of 197 km^3/yr of sea-ice, 97% of which is exported offshore across the western shelf break. Sabrina's high sea-ice production rate is well correlated (0.95) to divergent sea-ice motion within the interior of the shelf. In contrast, the Adélie Basin produces only 34 km^3/yr of sea-ice. Sea-ice productivity (production per unit area) in Sabrina Basin (4.6 m/yr) is comparable to the Ross Sea (4.5 m/yr), but still higher than the Adélie Basin (1.9 m/yr).

Based on the estimated contributions of salt, from sea-ice production, and freshwater, from both sea-ice and glacial-ice melt, the salinity evolution of a thick subsurface Thermostad Water layer is reconstructed for 2003–2015. A melt rate of 157.5 Gt/yr in the Totten Glacier and Moscow University Ice Shelf system is required to match the Thermostad Water salinities measured during the summers of 2014 and 2015.

Shelf Water ($S > 35.52$) was initially produced during the winters of 2003-2008. SW formation stopped, however, during 2008-2011 when summer sea-ice divergence and cross shelf break export (~10 km^3) were at a minimum, which resulted in a prominent Thermostad Water freshening of -5.07 ΔS per decade. In contrast, large summer sea-ice exports (>30 km^3) since 2011 have significantly increased the Thermostad Water salinity at a rate of 2.16 ΔS per decade. Thus, it is projected that local Antarctic Surface Water will form Shelf Water again by 2017, and the Sabrina Basin could participate more actively in the global Meridional Overturning Circulation than it has during the past decade.

ACKNOWLEDGEMENTS

It is bittersweet writing this because it signifies the end of an era for myself, a time that began Fall 2010, when I started coursework at Texas A&M University. Almost seven years later, I can now fully comprehend what this institution has done for me. It has provided me an unparalleled education, lifelong friendships, a love for tradition, jobs, and ultimately the woman I am going to marry. While I could produce a seemingly never-ending list of the positives, it is worth noting the hardships that I have endured while in school as well. I have overcome the passing of a grandfather, rigorous coursework including three fluid dynamics courses, being away from family and friends, and losing money because the Fightin' Texas Aggie football team never could quite put it all together. Some of these battles may not seem as important, but I can assure you that they seemed that way at the time. The last battle that I faced was this thesis. My pursuit of a graduate degree was filled with ups and downs, peaks and valleys, but thanks to a crew of supportive family, friends, mentors, and Netflix series in Spanish, I was able to stick the course and see it through.

I would like to start with thanking my friends. Clif and Jacob were basically my roommates for my entire time spent in college and I cannot imagine what this time in my life would be like without them. Through thick and thin, I could always count on them to be there at the end of the day to pick me up, dust off my shoulders, and put a smile on my face.

My family and friends back home always provided me with an escape and words of encouragement when College Station became a little too much to handle. While I was not always the best at constantly staying in touch with my friends, when I returned, it was as if nothing had skipped a beat, and they were the ones who found out about the important happenings first. My mom, dad, and sister lent an ear and offered tips from their experience whenever I needed. It is because of them and the way I was brought up that I have become the man that I am today. I am not perfect, but I am in a great place thanks to them.

Thirdly, I would like to thank the members of the Southern Ocean Research Group, my advisor, Dr. Orsi, and my officemate, Natalie. We have seen most likely every hour of the day together at some point during this journey. While it was not always fun, we stuck together. We conquered technology mishaps, messy data, quickly approaching deadlines, graduate school funding, MATLAB, and our hunger for bagels and coffee, and typically in every meeting we had. Dr. Orsi and Natalie provided me with a home away from home that at the very least supplied my life with the memories that make for great stories.

I could not have made it to the end if it were not for my fellow oceanography graduate students. We partied, studied, baked, and propped each other up. We celebrated graduations, holidays, weddings, and always made sure that we were all taken care of. Graduate school is tough, so I am grateful I had such a strong group of colleagues to keep me going.

Finally, I would like to thank my graduate school sweetheart turned wife, Luz. Schedules do not really exist in graduate school, but she always found time to listen to me, ease my mind, introduce me to new things, and be the partner that I know I can take on anything with. The completion of this degree marks an end of one journey, but also the beginning of my next, and I am thrilled to have found someone who I can cherish the positives and overcome the challenges with. Gracias y te amo.

CONTRIBUTORS AND FUNDING SOURCES

This work was supervised by a thesis committee consisting of Professor Alejandro Orsi and Professor Achim Stoessel of the Department of Oceanography and Professor Nielsen-Gammon of Atmospheric Sciences. Graduate study was supported by National Science Foundation grants, the Scherck Fellowship, and a teaching assistantship through the Department of Environmental Programs at Texas A&M University.

NOMENCLATURE

AABW	Antarctic Bottom Water
AASW	Antarctic Surface Water
ACC	Antarctic Circumpolar Current
ASF	Antarctic Slope Front
CDW	Circumpolar Deep Water
MCDW	Modified Circumpolar Deep Water
MSW	Modified Shelf Water
SW	Shelf Water
ThW	Thermostad Water
TG-MUIS	Totten Glacier – Moscow University Ice Shelf

TABLE OF CONTENTS

Page

LIST OF FIGURES

Page

LIST OF TABLES

Page

1. INTRODUCTION

Heat, salt and freshwater are effectively redistributed only over certain segments of the Antarctic continental shelf, but these air-sea-ice interactions influence property distributions in the rest of the World Ocean [*Deacon*, 1937]. At some sites, e.g. as shown in **Figure 1**, upper waters are transformed into relatively denser waters that supply the lower branches of the global Meridional Overturning Circulation.

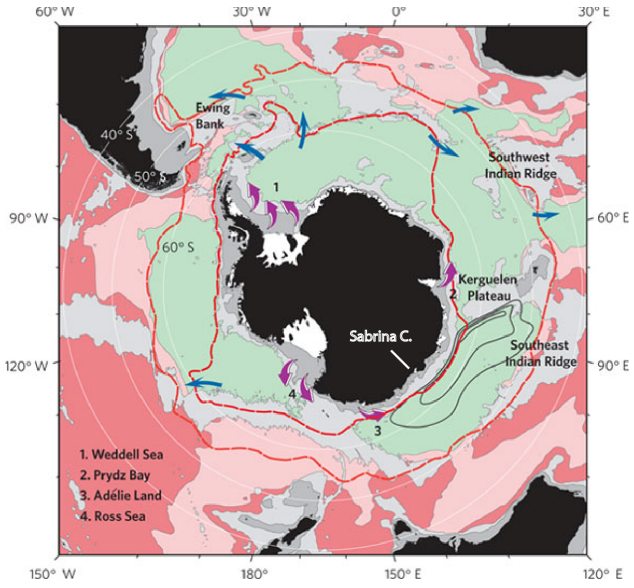

Figure 1. Schematic of the Southern Ocean circulation. Relevant features in the schematic are as follows: Purple arrows indicate outflow of new AABW to the deep ocean. Blue arrows indicate northward pathways of AABW. Bottom waters with neutral density greater than 28.27 kg/m^3 are green and red is less than 28.20 kg/m^3. Figure adapted from [*Orsi*, 2010].

Sea-ice forms over the continental shelf when sufficient heat is lost by Antarctic Surface Water (**AASW**; $\theta > -1.9$ °C; $\gamma^n < 28.00$ kg/m^3) to the atmosphere. This sea-ice is ultimately carried offshore by surface currents (**Figure 2**). Coastal polynyas are shelf areas with persistently open waters in the winter, and are often referred to as 'salt factories' because of their high sea-ice productivity. Polynyas are the most likely sites where AASW is transformed into the much denser, saltier and near-freezing Shelf Water (**SW**; $\theta < -1.9$ °C; $\gamma^n > 28.27$ kg/m^3; $S > 34.52$), which sinks to the bottom layer of shelf troughs [*Gill*, 1973]. The Ross and Weddell seas are the major SW sources because enhanced sea-ice formation is expected to take place within their vast coastal polynyas. The relatively smaller Prydz Bay and Adélie Coast coastal polynyas are also well-documented sites of SW production and export of new local types of AABW [*Orsi et al*., 1999; *Rintoul*, 1998; *Gordon and Tchernia*, 1972].

Relatively warm ($\theta > 1$ °C), saline ($S > 34.65$), and oxygen-poor ($O_2 < 4.5$ ml/l) Circumpolar Deep Water (**CDW**) is transported eastward by the Antarctic Circumpolar Current (**ACC**), and it only overrides the Antarctic shelf break (**Figure 1**) in the Bellingshausen Sea and Drake Passage **[***Orsi et al*., 1995]. Elsewhere, either large subpolar gyres distance the ACC from the coast, e.g. in the Atlantic and western Pacific sectors, or its southern boundary extends approximately along the foot of the continental slope.

The Antarctic Slope Front (**ASF**) is a sharp subsurface property gradient (**Figure 3**) separating typical water mass structures of the oceanic and shelf regimes [*Whitworth et al.,* 1998]. It extends westward from the Amundsen Sea to the northwestern Weddell

Sea. All along this path CDW from the oceanic domain mixes with a thickened layer of AASW across the poleward-sloping isopycnals characteristic of the ASF (**Figures 2-3**) to form Modified Circumpolar Deep Water (**MCDW**). In some shelf regions MCDW enters the shelf and mixes with SW at the bottom layer to form Modified Shelf Water (**MSW**). On approaching the troughs sill MSW is able to spill down the continental slope, and below the ASF, entraining ambient CDW to form Antarctic Bottom Water (**AABW**).

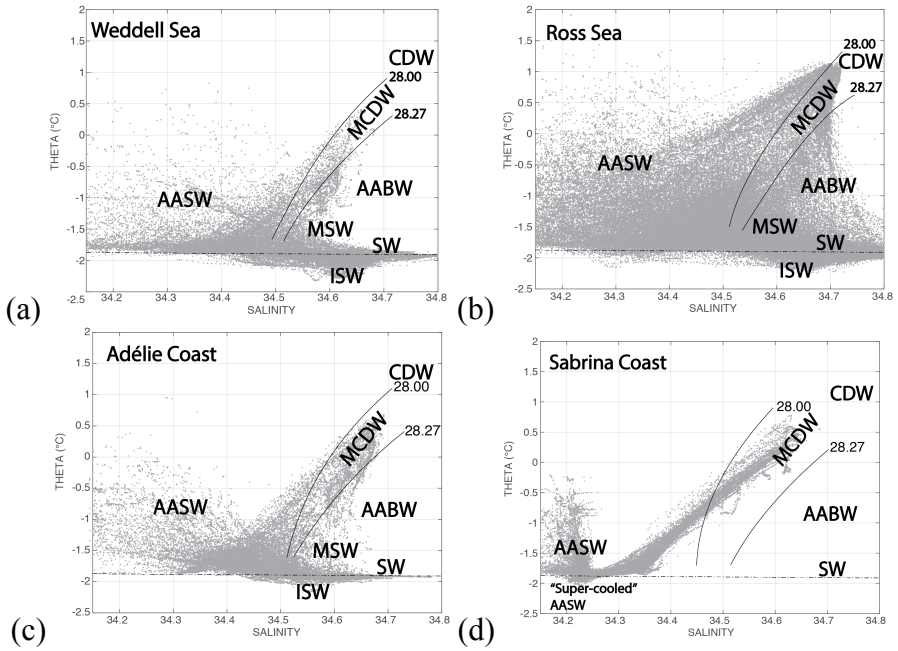

Figure 2. θ-S scatter plots from Southern Ocean Database stations in the (a) Weddell Sea, (b) Ross Sea, and off (c) Adélie, and (d) Sabrina coasts; the traces of 28.00 kg/m^3 and 28.27 kg/m^3 neutral density surfaces are shown with solid lines whereas the surface freezing point is indicated by the dash line.

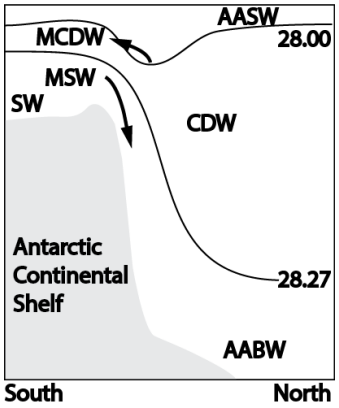

Figure 3. Schematic of water mass stratification at Antarctic slope locations producing new AABW.

1.1 Paradigm

Widespread and long-term freshening of both AASW and SW have been reported in the Ross Sea (-0.03 ΔS per decade) and in the Adélie Coast (-0.01 ΔS per decade) [*Jacobs*, 2006; *Jacobs et al*., 2002; *van Wijk and Rintoul*, 2014]. These are in apparent conflict with the reported decadal (2000-2011) trend of increased sea-ice thickness (18.4 cm per decade) in the Ross Sea [*Wiederwohl*, 2012]. To investigate this conflicting evidence one must first identify potentially unaccounted freshwater sources over particular segments of the continental margin, and ultimately reproduce the observed environmental evolution incorporating estimates of both local sea-ice production and freshwater inputs.

Sea-ice volume within a particular shelf embayment may increase due to contributions of sea-ice formed in coastal areas farther upstream or offshore, but local upper waters would not gain any salt from this type of interior sea-ice growth. Net exchange of sea-ice volume across the shelf break segment spanning this embayment yields how much volume is actually produced or melted within the “gate”, which in turn

would rise or lower surface waters salinity. Also, when the pack-ice motion inshore is divergent (convergent), it is more (less) likely for the basin to export sea-ice. An increase (decrease) in interior sea-ice volume that is not accounted for by cross-gate exchange must result from the local sea-ice growth (melt). Therefore, maximum brine rejection to local surface waters is expected during times of large sea-ice export and interior sea-ice growth.

Significant freshwater contributions to the AASW layer result from basal and lateral melt of surrounding floating ice shelves and glaciers. This influence strengthens the stability of local stratification by reducing the salinity of upper waters. Unlike in the Adélie Basin, the melting of relatively larger and more unstable glaciers and ice shelves in the Sabrina Basin can potentially overshadow the convective potential of sea-ice formation by preventing SW formation.

1.2 Case Study

Although the area (~43,000 km^2) and volume (~25,500 km^3) of the embayment off the Sabrina coast (118°E) are much larger (2.5 and 3 times) than off Adélie (144°E); both shelf segments have some geographic characteristics in common (**Figure 4**). They are bounded by prominent icescapes: to the east by the Dalton Iceberg Tongue, and the Mertz Glacier Tongue; and to the south by the TG-MUIS, and the Ninnis and Mertz glaciers. Mertz Glacier Tongue broke off in 2010 when iceberg B9B collided with it.

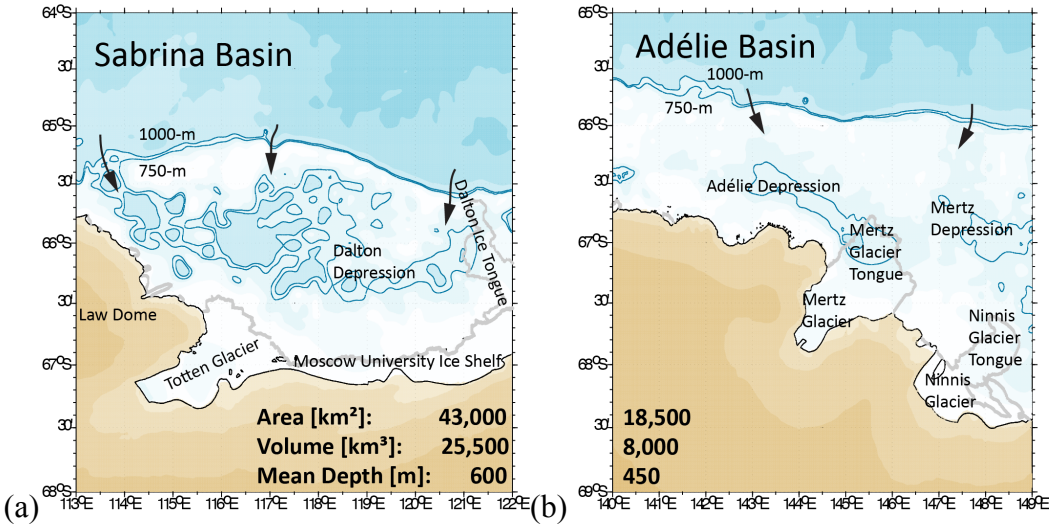

Figure 4. Location maps of (a) Sabrina and (b) Adélie basins, with the most prominent geographic and bathymetric features labelled. Black arrows indicate the sills of shelf troughs, where the deepest oceanic inflows can cross the shelf break.

Basal melt rate estimates (**Table 1**) for TG-MUIS (90.6 Gt/yr) are considerably higher than for Mertz and Ninnis glaciers (10.1 Gt/yr) [*Rignot and Jacobs*, 2013].

Table 1. Basal melt rates at key Antarctic locations as reported by *Rignot and Jacobs* [2013].

Region	Basal Melt Rate [Gt/yr]
Totten Glacier	63.2 ± 4
Moscow University Ice Shelf	27.4 ± 4
Mertz Glacier	7.9 ± 3
Ninnis Glacier	2.2 ± 3

The area of the Dalton (~5,500 km^2) polynya is about four times smaller than the Mertz (~23,500 km^2) polynya [*Massom et al.*, 1998], but the latter shrunk after the B9B collision with Mertz Glacier Tongue in 2010.

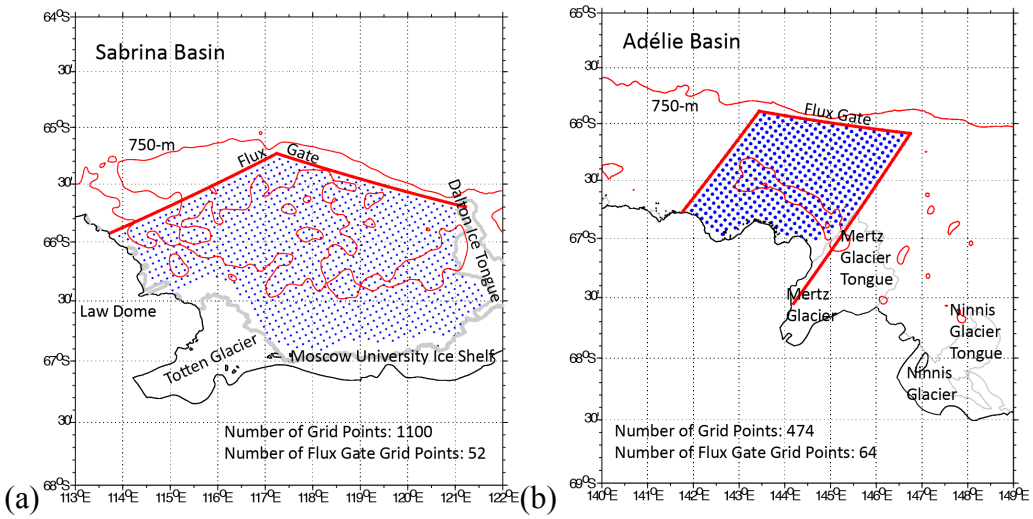

Figure 5. Distribution of the (a) 1,100 working grid points over the Sabrina Basin and (b) the 474 working grid points over the Adélie Basin; the thick red lines indicate the sea-ice flux "gates" used to calculated bi-weekly exchanges.

Waters filling the bottom layer of cross-shelf troughs in the Sabrina and Adélie embayments only have access to the oceanic domain along multiple narrow gaps near the shelf break. Their locations are indicated by the black arrows in **Figure 4** nearly along the 750-m isobath at about 114°E, 117°E, and 121°E in the Sabrina Basin and 143°E and 148°E in the Adélie Basin. Whereas intrusions of relatively warm ($\theta > 0.5$ °C) MCDW provide heat and salt to the Adélie Basin, only relatively warm ($\theta > 0$ °C) Thermocline Water from the slope regime enters at the eastern Sabrina Basin (**Figure 2c, d**).

Available measurements of salinity and potential temperature near the continental ice fronts indicate significant meridional exchange of waters, and active interaction of currents with the seafloor and undersides of floating glaciers and ice shelves (**Figure 2c, d**). Whereas near-freezing SW melts the base of Mertz Glacier, a

much fresher Thermostad Water (**ThW**, ~ -1.8 °C) continues poleward under the TG-MUIS.

In the Sabrina Basin, the void in θ-S space at S > 34.52, γ^n > 28.27 kg/m^3, and θ < -1.85 °C indicates that lack of local SW. Therefore, unlike in the Mertz Basin, sea-ice formation within the Dalton Polynya does not appear to destabilize the water column, or overcome the counter effect from local freshwater sources in the TG-MUIS system.

2. DATA

This study analyzes all available in-situ and remote measurements of sea-ice fields and atmospheric forcing for the 2003-2016 timeframe in the Sabrina Basin, East Antarctica. Sea-ice concentration (C) is obtained from the University of Bremen Institute of Environmental Physics [*Spreen et al*., 2008], for 2003-2016 at the highest spatial (6.25-km; polar stereographic projection) and temporal (daily) resolutions. The sea ice concentrations in this dataset were derived from observations from passive microwave sensors that can detect and classify sea-ice based on its brightness temperature.

Sea-ice thickness, $H = (C_1 / 100) * S_1 + (C_2 / 100) * S_2 + (C_3 / 100) * S_3$, is calculated following *DeLiberty et al*. (2004), based on data on the stage of development (S) of three distinct classifications (thickest, middle, and thinnest) provided by the United States National Naval Ice Center (USN-NIC). This biweekly data set incorporates in-situ, radar, and remote sensing data sources. Nevertheless, a direct comparison to vessel-based measurements from the Antarctic Sea ice Processes and Climate (ASPeCt) program found the estimated H time series to overestimate by about 48% [*Morgan*, 2011].

Sea-ice motion is provided by the National Snow and Ice Data Center (NSIDC), for 2003-2015 with daily and 25-km resolutions. These motion fields represent a composite of data from various sensors with unique temporal resolutions [*Tschudi et al*., 2016]. Wind velocity (10-m) and air temperature (2-m) data derived from by the

European Centre for Mid-Range Forecasts (ECMWF) ERA-Interim reanalysis, for 2003-2016 at 6-hr intervals and 1/8° grid spacing. Hydrographic data was collected with an Underway CTD system during the first cruises to the Sabrina Basin: in 2014 by the U.S. (NBP1402) and in 2015 by Australia (AU1402).

Quantitative analyses of source time series with different temporal and spatial resolutions were simplified by projecting onto 6.25-km polar stereographic grids for the Sabrina and Mertz regions (**Figure 5**). Parameters involving sea-ice thickness were averaged to its coarser bi-weekly intervals. Missing data were filled using nearest neighbor spatial interpolation. If no neighbor was available, data were linearly interpolated in time.

3. ENVIRONMENTAL SEASONALITY

Two seasons are considered in this study, namely the austral summer (December-March) and the austral winter (April-November), while computing record-length mean seasonal properties maps shown in **Figure 6**.

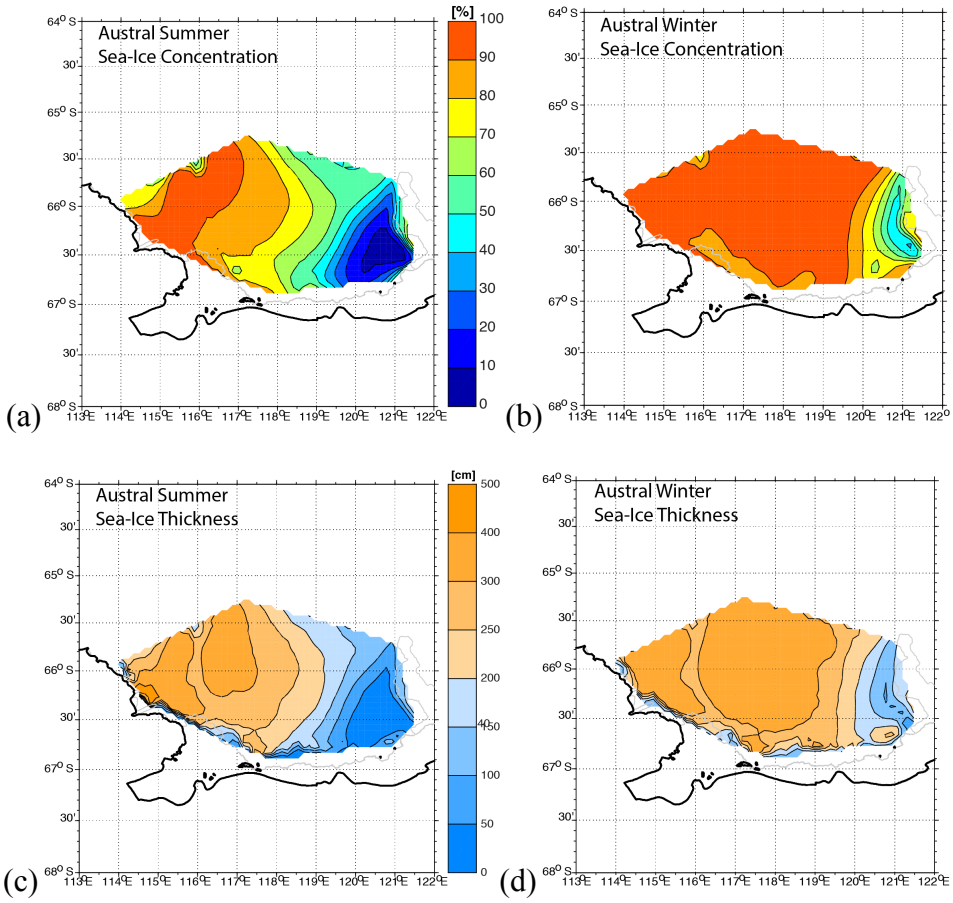

Figure 6. Maps of mean austral summer (left) and winter (right) properties: (a, b) sea-ice concentration, (c, d) sea-ice thickness, (e, f) sea-ice motion, (g, h) sea-ice divergence, (i, j) air temperature, (k, l) wind velocity, and (m, n) wind stress curl.

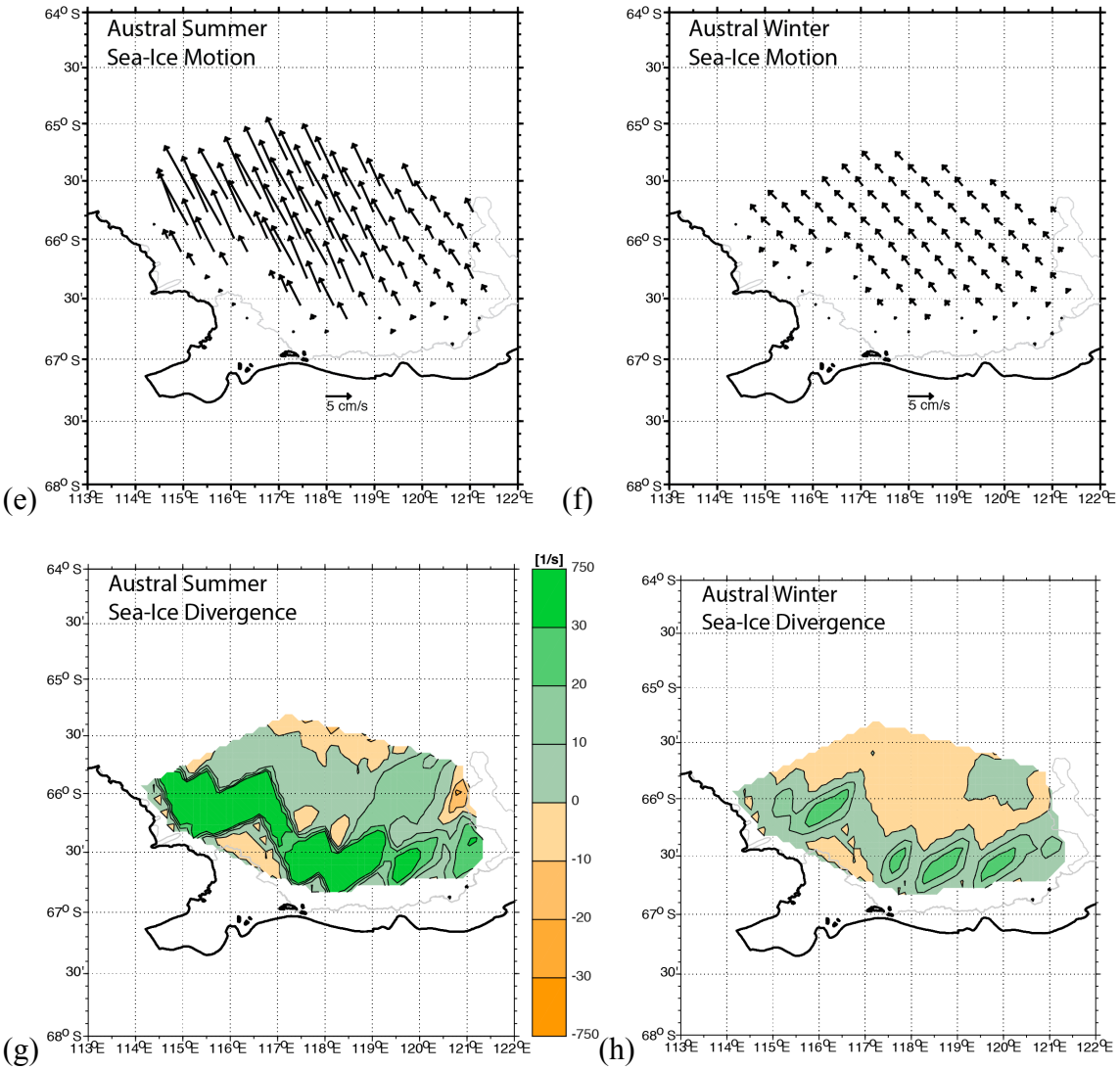

Figure 6. Continued

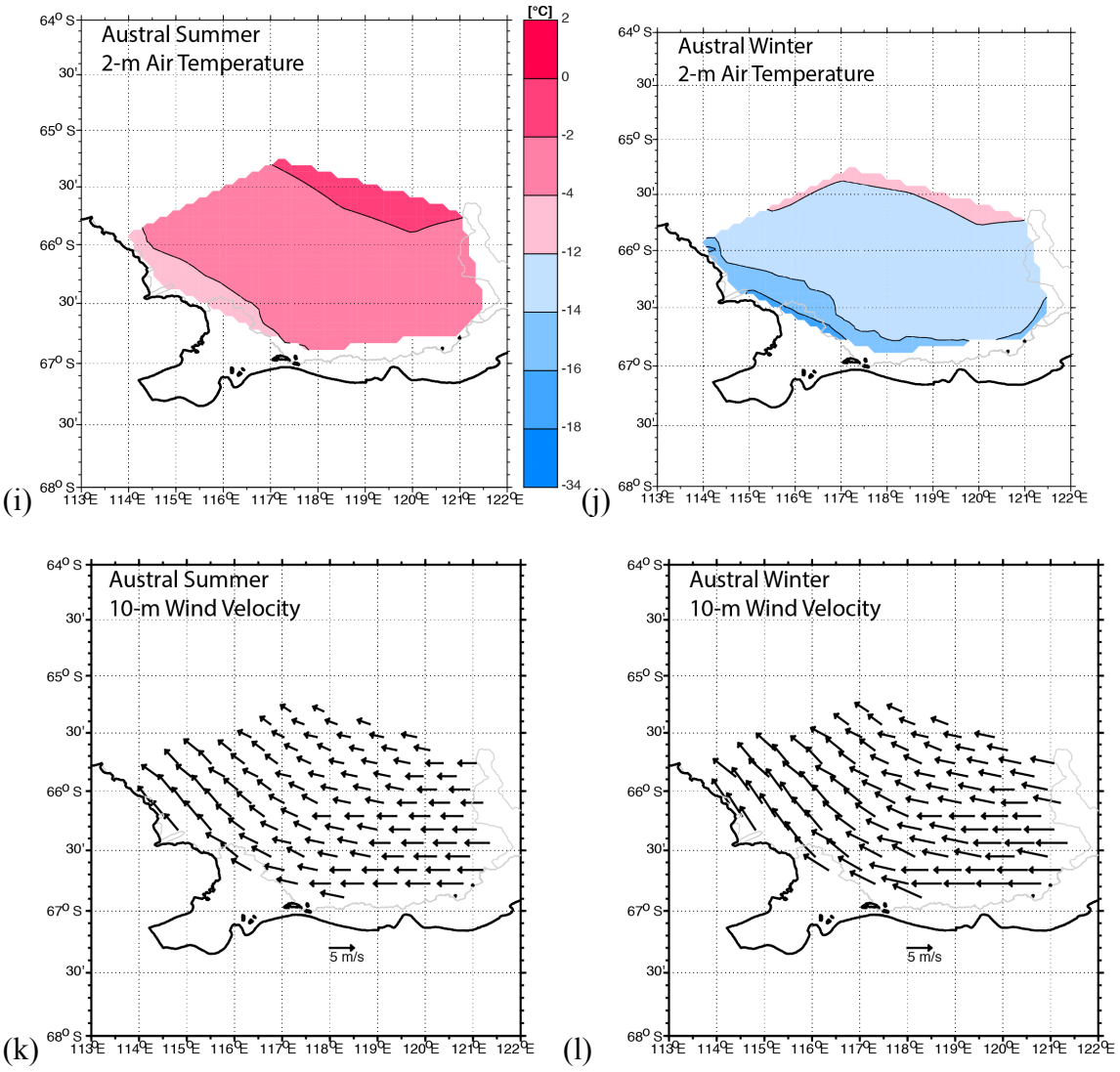

Figure 6. Continued

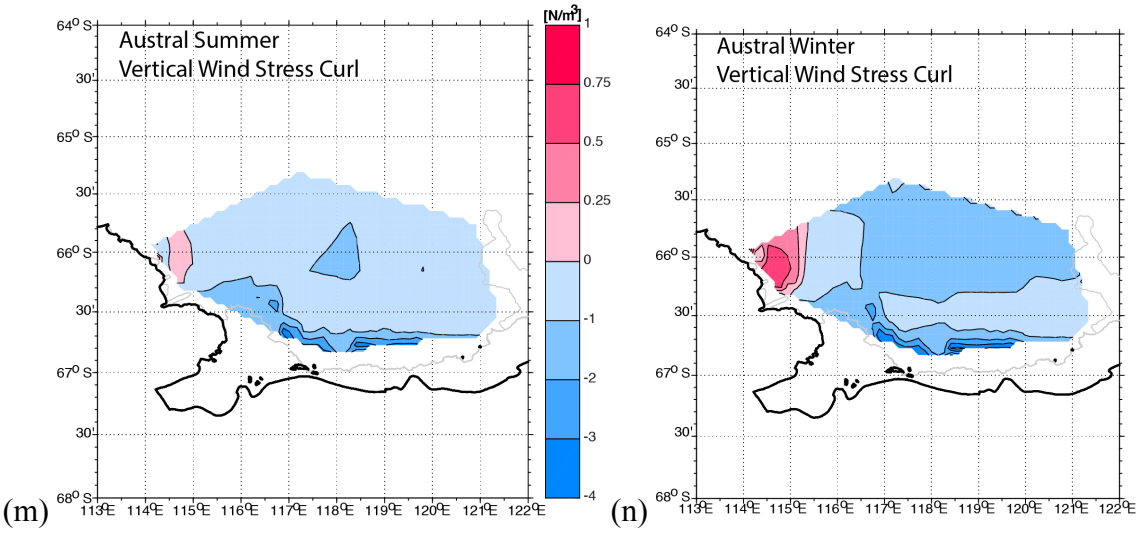

Figure 6. Continued

Summer sea-ice conditions are characterized by heavy ice (C > 90% and H > 250 cm) west of 117°E, and relatively open areas (C < 40% and H < 100 cm) east of 120°E (**Figures 6a and 6c**). Except for a very narrow band in front of TG-MUIS, heavy-ice areas expand to about 120°E in the winter (**Figures 6b and 6d**), whereas the eastern basin still shows relatively low concentrations (C < 70%) and thicknesses (H < 200 cm) where new sea-ice is likely formed. Moreover, there is no apparent interannual variability in the area occupied by the eastern interior and southern coastal polynyas.

Summer sea-ice motion is predominantly to the northwest all year long (**Figures 6e-f**) but it is intensified in the summer, with speeds greater than 5 cm/s near the shelf break. In contrast, the winter export of relatively thick pack-ice takes place at much slower speeds. Enhanced summer cross-shelf break export of sea-ice volume produced within Sabrina Basin during the previous winter is confirmed by the seasonal pattern of

sea-ice diverge shown in **Figures 6g-h**. Sea-ice motion within the basin is mostly divergent (> 0) in summer, but the winter convergence found over areas well inshore of the shelf break leads to ridging and thickening of pack-ice to as far south as 66.5°S. The inner shelf farther to the south remains divergent all year round and newly-formed winter sea-ice moves northward toward the convergent outer shelf region.

Atmospheric conditions in the Sabrina Basin vary greatly between seasons. Summer surface air temperatures (**Figures 6i-j**) are above -3 °C with only slightly cooler (< -4 °C) areas near Totten Glacier and Law Dome. Winter temperatures fall to -13 °C, and the coldest (-20 °C) coastal band reflects the influence of dense continental air drainage. This results in the largest air-sea surface temperature gradient during the winter, which in turn fuels sea-ice formation within coastal polynyas.

A cyclonic pattern of surface winds in the Sabrina Basin is observed in both seasons, roughly following the shape of the coastline, but intensified during the winter (**Figures 6k-l**). While in the open ocean winds effectively steer surface currents and the drift of sea-ice, in coastal areas it is the distribution of prominent underlying topography that controls their paths. Only west of about 117°E the fields of sea-ice motion and surface winds show similar paths, whereas a significant sea-ice drift (~ 45°) to the northwest of prevailing easterly surface winds is indicated over the eastern half of the basin. Surface wind stress curl distributions (**Figure 6m-n**) indicate that the basin is mostly characterized by upwelling (< 0) of subsurface waters, with relatively stronger values in front of TG-MUIS.

4. DECADAL TRENDS IN ENVIRONMENTAL CONDITIONS

The 2003-2016 time series of regional property averages for the Sabrina Basin are analyzed to detect interannual to decadal variability (**Figure 7**). Their main statistics are listed in **Table 2**. Although sea-ice concentrations (1.6% per decade in **Figure 7a**) and surface air temperatures (-0.13 °C per decade in **Figure 7f**) remained relatively constant, sea-ice thickness (-26.79 cm per decade in **Figure 7b**) decreased substantially and pack-ice divergence (0.97 s^{-1} per decade in **Figure 7e**) increased over the years. Thus, atmospheric warming is ruled out as the driver for the observed sea-ice thinning.

A 0.76 m/s per decade weakening of westward speeds and 0.3 m/s per decade strengthening of northward speeds (**Figure 7g, 7i**) indicate a regional pattern trending toward more southerly winds. This in turn supports a potential increase in the sea-ice volume exported cross the shelf break. At the estimated rate of change in surface wind stress curl of 0.2 N/m^3 per decade (**Figure 7h**), the predominant upwelling regime in Sabrina Basin may become characterized by downwelling in the next decade or so. Surface wind stress curl distributions (**Figure 6m-n**) show that the basin is mostly characterized by upwelling (< 0) of subsurface waters, with relatively stronger upwelling indicated in front of TG-MUIS.

Fairly constant low air temperatures (-9.47 °C) found over a continental shelf that is covered with progressively thinner sea-ice implies that surface waters in the Sabrina Basin had a potentially greater exposure to atmospheric forcing during this period of

time. As larger areas of open waters develop in the summer a greater portion of the shelf becomes available to produce sea-ice at the beginning of the winter. In turn, a relatively larger salt rejection could lead to SW production in the near future. However, little is known about the combined effect of multiple local freshwater sources. A thorough account of sea-ice production and freshwater inputs to the Sabrina Basin is, therefore, warranted to fully understand the regional water mass characteristics, their variability and role in the Meridional Overturning Circulation.

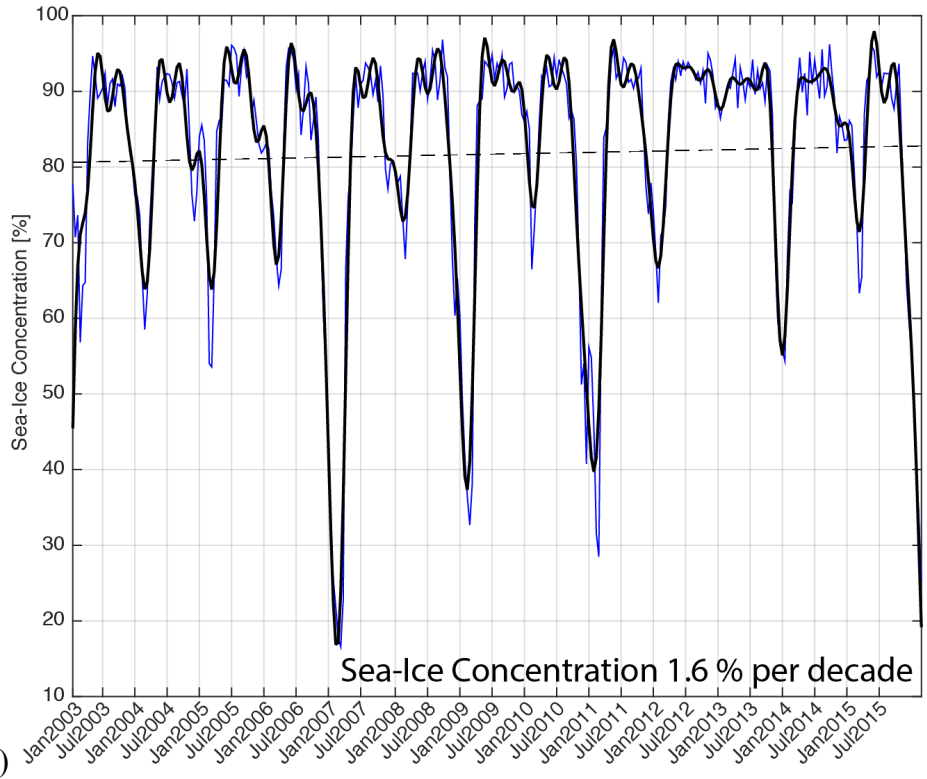

(a)

Figure 7. Daily (blue) and filtered (8-week Lanczos Low Pass, black) time series of shelf-averaged properties, and their linear fits (dashed lines): (a) sea-ice concentration, (b) sea-ice thickness, (c) sea-ice zonal motion, (d) sea-ice meridional motion, (e) sea-ice divergence, (f) air temperature, (g) zonal wind speed, (h) meridional wind speed, and (i) wind stress curl.

(b)

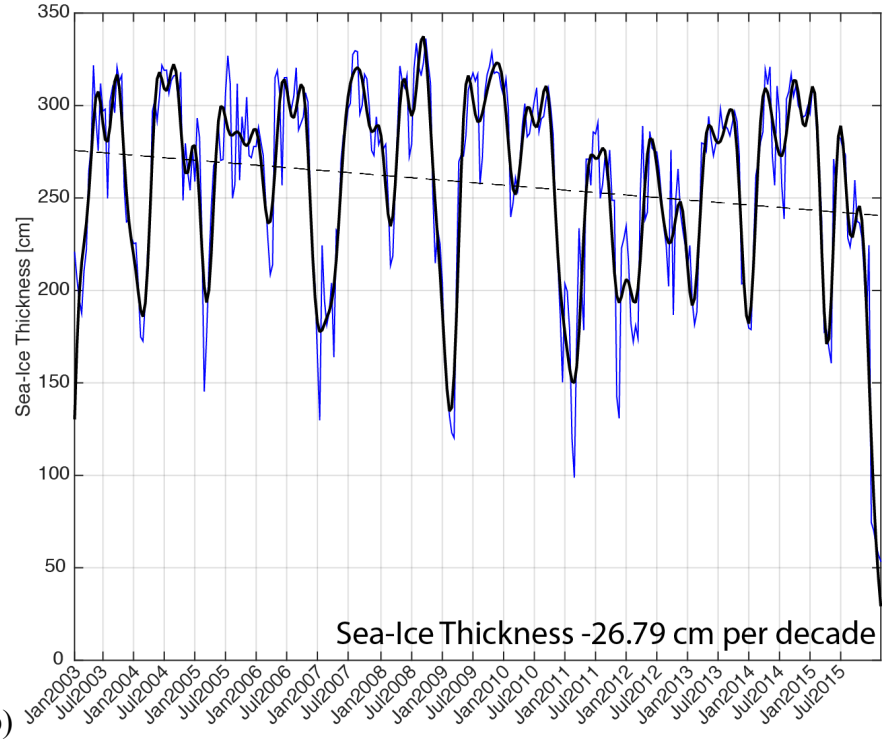

(c)

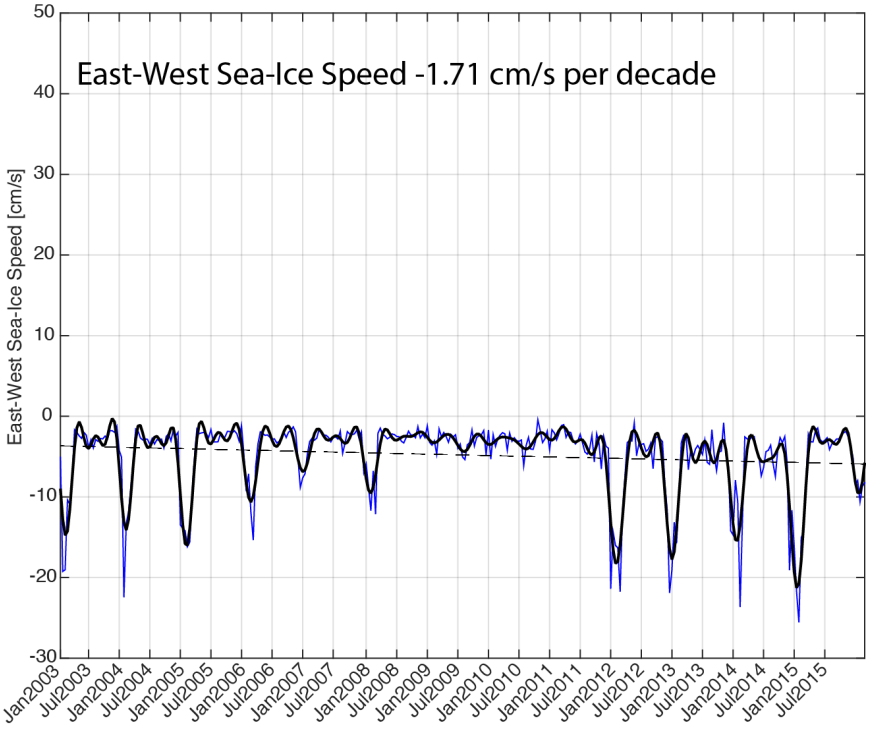

Figure 7. Continued

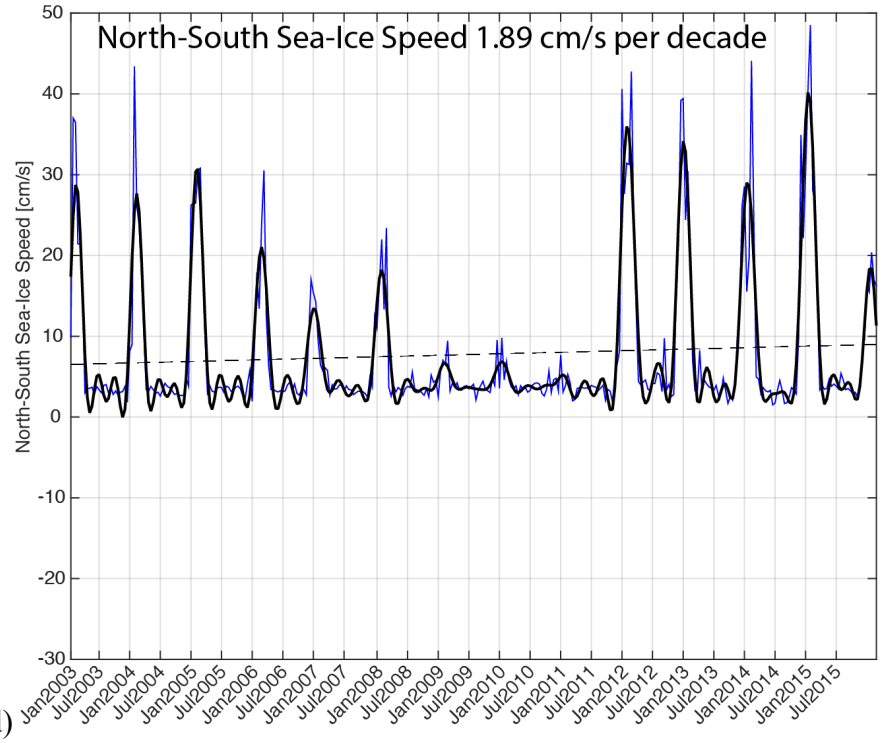

(d)

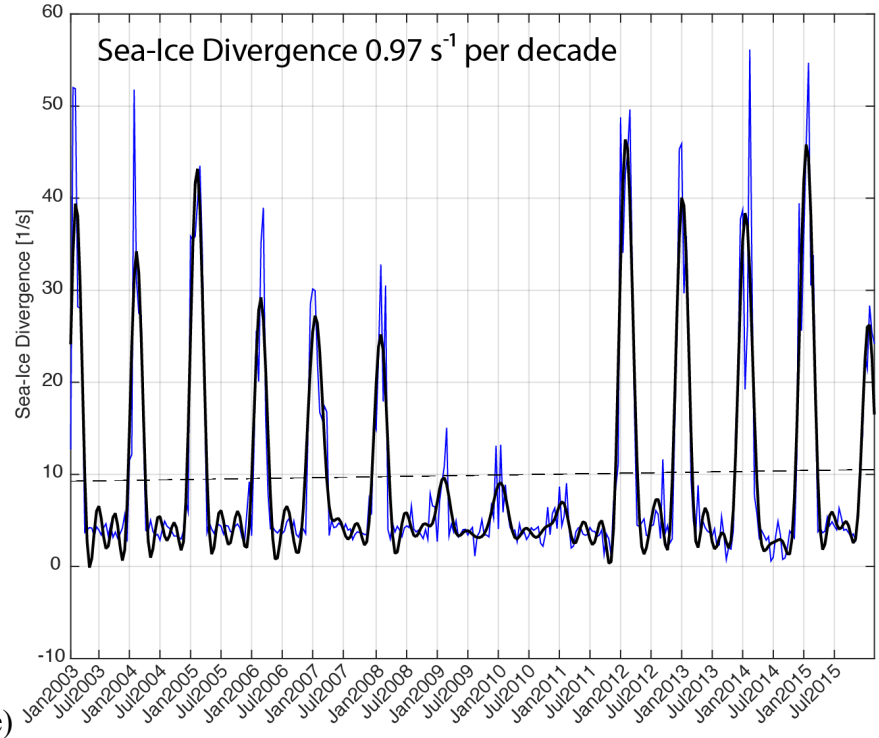

(e)

Figure 7. Continued

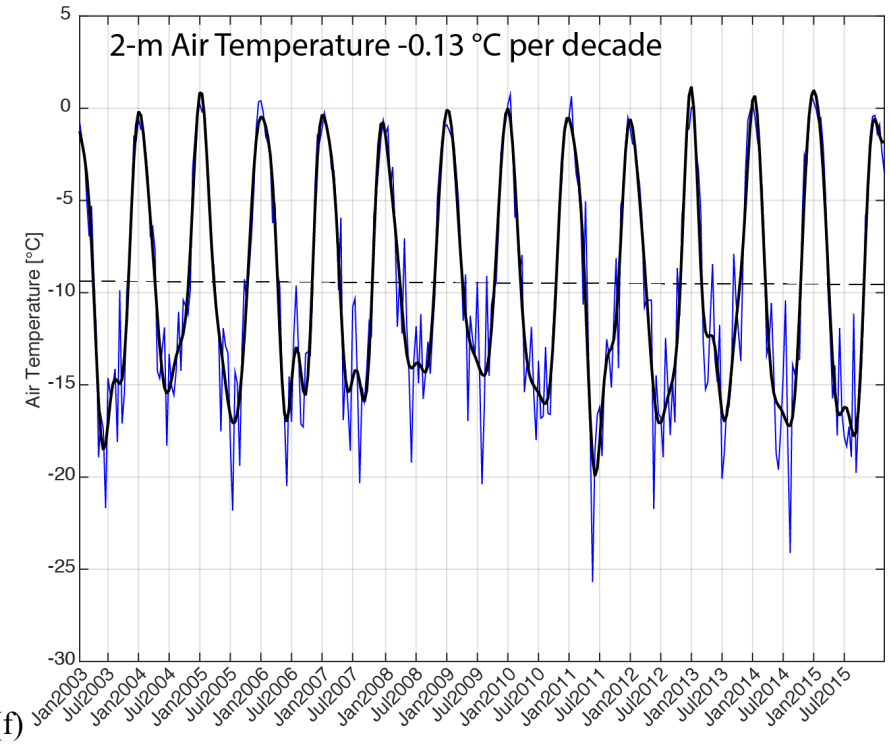

(f)

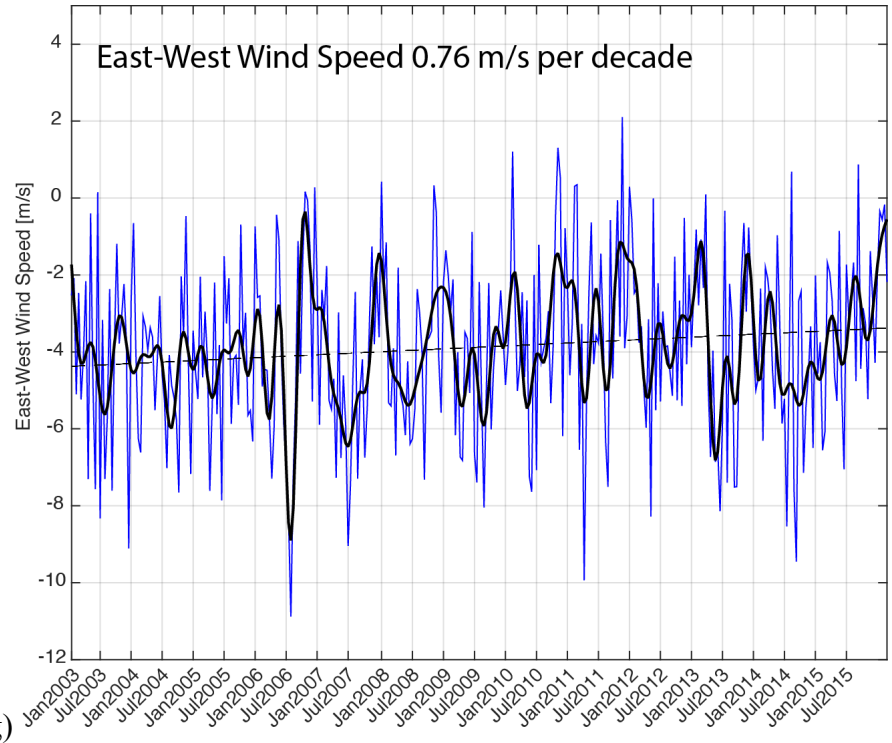

(g)

Figure 7. Continued

(h)

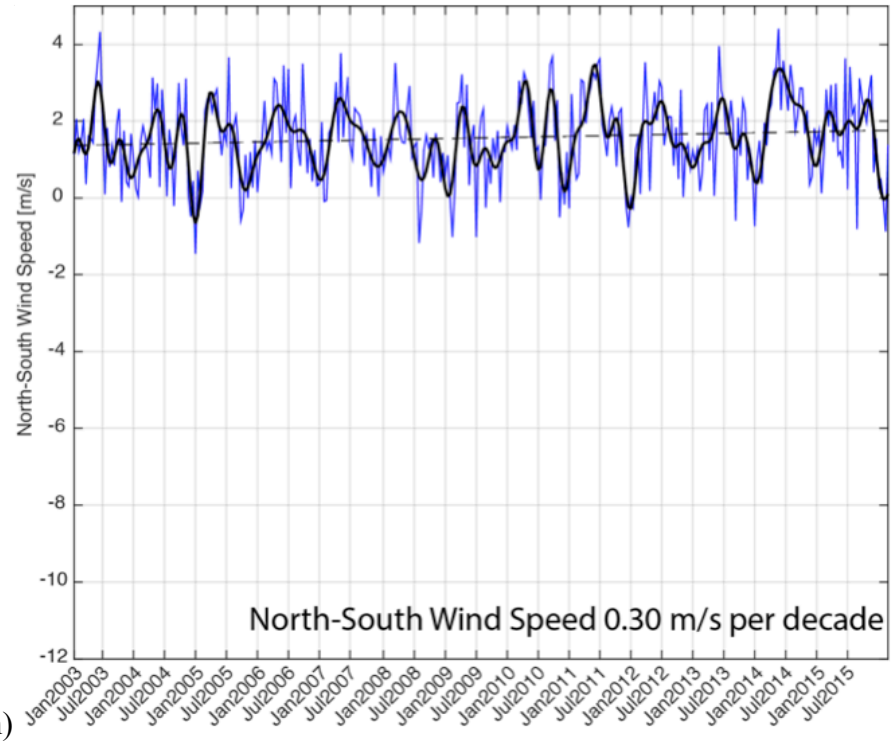

(i)

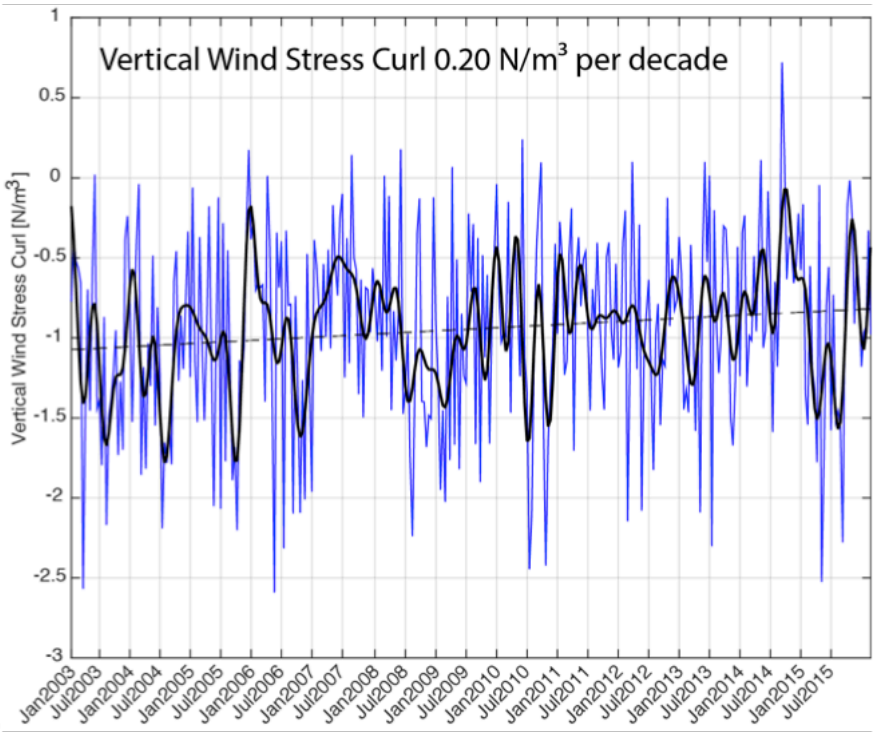

Figure 7. Continued

Table 2. Statistics of regionally-averaged parameters in the Sabrina Basin.

	Minimum	Maximum	Mean	Decadal Trend
Sea-Ice Concentration [%]	16.59	96.83	81.83	1.6
Sea-Ice Thickness [cm]	53.63	336.20	258.42	-26.79
E-W Sea-Ice Motion [cm/s]	-25.55	-0.43	-4.81	-1.71
N-S Sea-Ice Motion [cm/s]	1.51	48.52	7.78	1.89
Sea-Ice Divergence [s^{-1}]	0.60	56.14	9.94	0.97
Air Temperature [°C]	-25.70	0.74	-9.47	-0.13
E-W Wind Speed [m/s]	-10.88	2.10	-3.88	0.76
N-S Wind Speed [m/s]	-1.46	4.41	1.57	0.30
Wind Stress Curl [N/m^3]	-2.59	0.72	-0.95	0.20
Wind Divergence [s^{-1}]	-2.27	0.37	-0.76	0.17

5. SEA-ICE PRODUCTION

Time series (biweekly) of sea-ice production rates within the Sabrina and Adélie basins are estimated taking advantage of high-resolution (6.25 km) data sets of sea-ice thickness and motion (**Figure 5**). The region's production rate is calculated as the sum of the net sea-ice volume transport across the shelf's nominal outer boundary [*Kwok and Rothrock*, 1999; *Kwok*, 2005; *Comiso et al*., 2011], and the variability of the remaining sea-ice volume (ΔVol) farther inshore. Each of these two terms can be positive or negative during any given time step, i.e. a net sea-ice export or import across the shelf break and an expansion or shrinkage of the sea-ice volume inshore, but there are only three typical settings, as described with **Figure 8**.

Peak summer exports represent the most productive scenario. E.g. the export of 26.9 km^3 (**Figure 8a**) during January 17-31 of 2005 resulted in a production of 22.5 km^3 even when the interior shrunk by 4.4 km^3. Peak fall growths inshore constitute another productive scenario. E.g. the interior expansion of 40.7 km^3 (**Figure 8b**) during May 2-16 of 2011 dominated the production of 44.4 km^3 rather than export of 3.7 km^3. The least common scenario is dominated by spring shrinkage within the shelf. E.g. the interior shrinkage of 12.2 km^3 (**Figure 8c)** during November 29 – December 13 of 2010 resulted in the loss of 7.1 km^3 in spite of the export of 5.1 km^3.

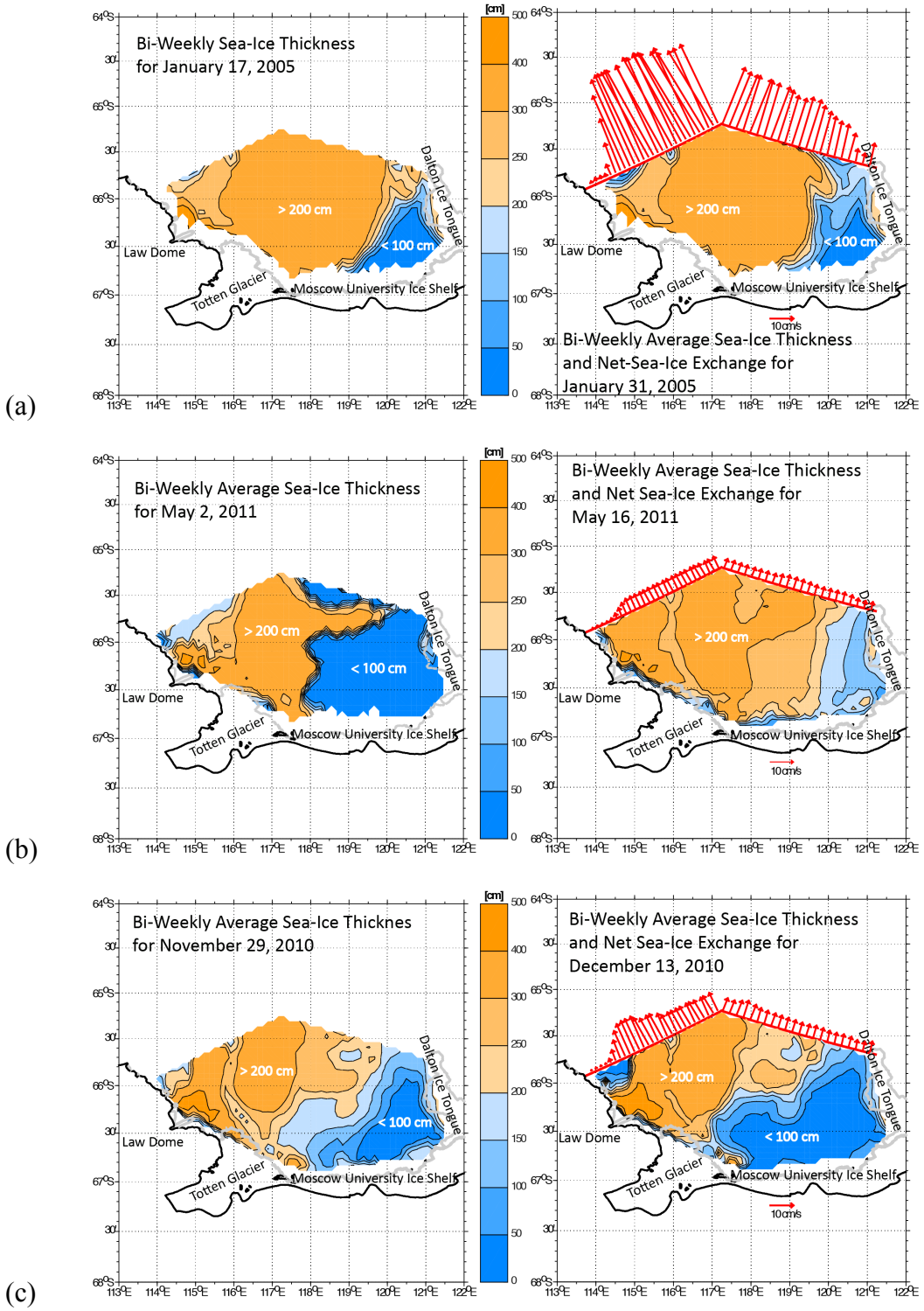

Figure 8. Distinct scenarios of sea-ice production: (a) summer export across the shelf break, (b) fall sea-ice pack growth within the shelf, and (c) spring shrinking of the interior sea-ice pack. Red arrows indicate sea-ice motion normal to the flux gate.

The estimated history of sea-ice production in the Sabrina Basin (**Figure 9**) shows relatively high summer rates (15 to 45 km^3) due to large exports (20 to 40 km^3) during 2003-2007 and 2012-2015. Similarly, the weak summer exports (5 to 20 km^3) during 2008-2011 and in 2015, combined with the loss of interior sea-ice volume (-5 to -15 km^3), resulted in minimum production rates (-5 to 10 km^3). During the fall, interior sea-ice volume grows and peaks (5 to 18 km^3) above waning exports (March-June) to still render moderate fall production rates (9 to 20 km^3).

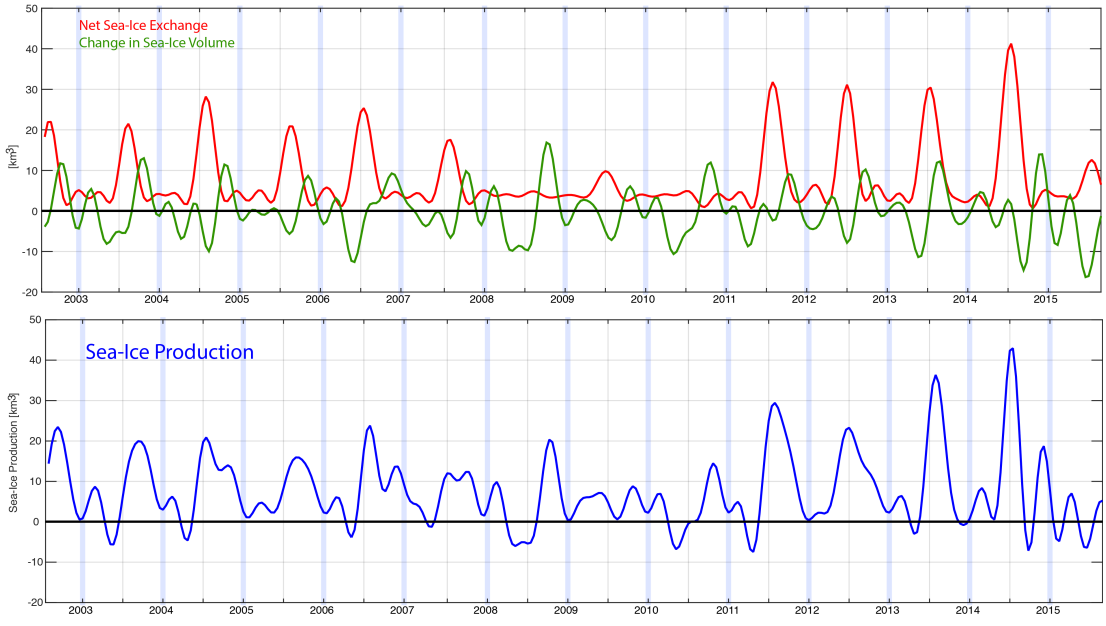

Figure 9. Time series of 16-week filtered (a) net sea-ice exchange across the shelf break (red) and change in interior sea-ice pack volume (green), and (b) sea-ice production (blue); vertical gridlines indicate the months of January (gray) and July (blue).

Winter sea-ice production is more positively correlated to the changes of interior sea-ice volume than to the net exchange of sea-ice volume across the shelf break (**Figure**

10). Regardless of the season, however, sea-ice production is highly (positively) correlated to both the interior sea-ice divergence and the net sea-ice export. This indicates that active winter air-sea interactions within the polynya, through breaking up and moving newly-formed sea-ice volumes away, effectively enhance subsequent summer exports.

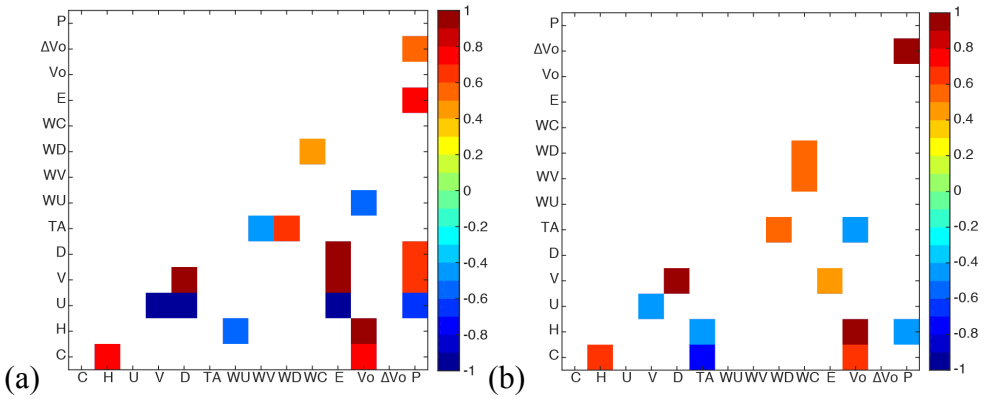

Figure 10. (a) Summer and (b) winter statistically significant (95% confidence level) correlation coefficients (> 0.4), after record-length means and linear trends were removed: sea-ice concentration (C) and thickness (H), zonal (U) and meridional sea-ice motion (V), sea-ice divergence (D), air temperature (TA), zonal (WU) and meridional wind speed (WV), wind stress divergence (WD) and curl (WC), net sea-ice volume exchange (E), sea-ice volume (Vo) and volume change (ΔVo), and sea-ice production (P).

6. REGIONAL SEA-ICE PRODUCTIVITY

Sea-ice production calculations using variable thickness and a constant thickness of 60 cm are compared regionally (**Table 3**). In all the scenarios, sea-ice exported offshore accounted to the bulk (92.6%–99.4%) of the production rates. A constant sea-ice thickness in the Ross Sea yields a production of 578.52 km^3/yr, of which the export across the shelf 'gate' is 74.18 km^3/yr larger than reported by *Comiso et al*., [2011]. Sea-ice production and productivity more than doubled (2.4 times larger) while taking advantage of the sea-ice thickness estimates introduced in this study. They are about four times as large in both the Sabrina and the Adelie basins.

Sabrina Basin's mean sea-ice production (197.41 km^3/yr) per unit area yields a sea-ice productivity of 4.6 m/yr, almost identical to the Ross Sea (4.5 m/yr) but more than twice the productivity of the Adélie Basin (1.9 m/yr). *Kusahara et al.* [2011] and *Tamura et al.* [2012] reported about ten times larger production rates for the Adélie Basin estimated here (34.38 km^3/yr).

Table 3. Sea-ice production [km^3/yr], contribution [%] of cross-shelf break exchange, and productivity [m/yr] for the Sabrina, Adélie, and Ross.

	Sabrina			Adélie			Ross		
H = 60 cm	47.69	98.42	1.11	8.49	92.58	0.46	578.52	99.25	1.86
Variable H	197.41	97.47	4.59	34.38	99.36	1.86	1397.64	97.70	4.50

7. SABRINA THERMOSTAD WATER SALINITY

A relatively thick subsurface layer (150-300 m) in the interior of the Sabrina Basin shows uniform temperatures (-1.8 °C) with values near the surface freezing point. The characteristics of this Thermostad Water (ThW) were first identified on summer CTD profiles (**Figure 11** and **Table 3**) from 2014 and 2015. They are reliable indicators of winter surface conditions when the ThW incorporates about 79% of the salt content in surface waters rejected during sea-ice formation [*Skogseth et al*., 2004].

Table 4. Characteristics of the thermostad layer observed in interior of the Sabrina Basin.

	2014 NBP1402	2015 AU1402
Salinity	34.26	34.27
Potential Temperature [°C]	__	-1.82
Density [kg/m^3]	__	1028.68

A prominent subsurface temperature minimum layer (100-400 m) with values well below the surface freezing point (< -1.9 °C) is found along a band in front of the TG-MUIS. This indicates that meltwater input from local continental sources influences the characteristics of the interior ThW layer in the Sabrina Basin. Reported basal melt rates combined with the new sea-ice production time series are used to calculate the mean salinity of the ThW layer, as:

Salinity = Mass Salt (seawater + rejected) / Mass (seawater + meltwater)

Even for the short span between the two cruises, neglecting freshwater input from glacial meltwater while progressively adding salt rejected by the estimated 184.81 km^3 of sea-ice produced during that time would increase the ThW salinity in 2014 by 0.7 by 2015; i.e. seven times larger than the observed salinity increase of 0.1 (**Table 3**). Estimated backwards from 2015 to 2003 (**Figure 12**), the ThW salinity would unrealistically increase over time at a rate of 5.55 ΔS per decade, contrary to the measured decadal freshening of upper waters around the Antarctic shelf.

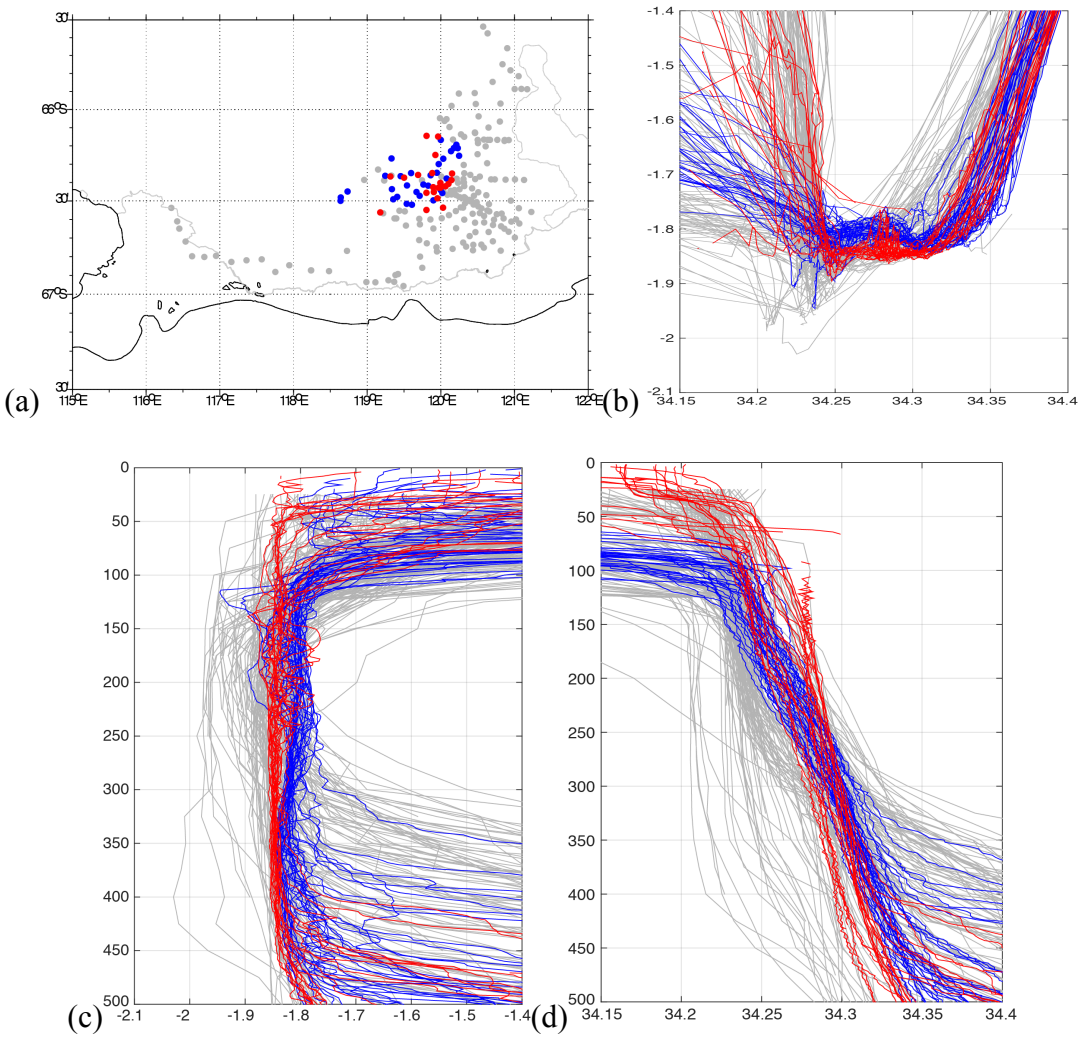

Figure 11. (a) Location of available stations in the Sabrina Basin, with blue (red) dots indicating a selection of interior stations from 2014 (2015), and their (b) θ-S diagrams, (c) θ profiles, and (d) S profiles.

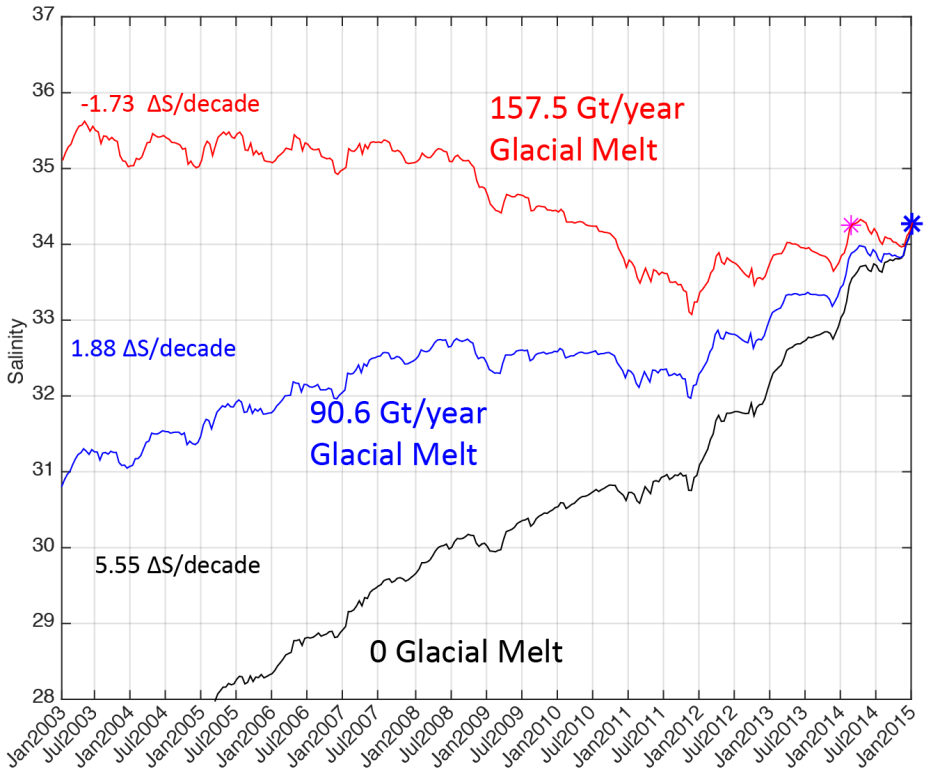

Figure 12. Time series of the salinity of the Thermostad Water layer estimated based on sea-ice production and different glacial melt rates: 0 Gt/yr (black), 90.6 Gt/yr (blue), and 157.5 Gt/yr (red). The blue (magenta) asterisk indicates the observed salinities in 2015 and 2014.

Calculating the evolution of the ThW salinity using the most recent TG-MUIS melt rate of 90.6 Gt/yr [*Rignot and Jacobs*, 2013] still results in a net salinification of the Sabrina Basin interior at a rate of 1.88 ΔS per decade. A glacial meltwater input of 157.5 Gt/yr between the two cruises not only reproduces the observed ThW salinities of 2014 and 2015, but also results in an overall freshening rate of -1.73 ΔS per decade. It is much larger than the reported glacial melt rates of this region (75%) and for the Pine Island Glacier (101.2 Gt/yr), but similar to the 144.9 Gt/yr reported for the Getz Ice Shelf [*Rignot and Jacobs*, 2013].

The estimated 2003-2015 evolution of the ThW salinity shown in **Figure 13a** suggests three distinct regimes. During the initial period of 2003 to June 2008 the relatively large summer exports (> 25 km^3; **Figure 13c**) of winter produced sea-ice volumes resulted in very high salinities (> 35) characteristic of SW. Afterwards, between July 2008 and November 2011, SW production in the Sabrina Basin was suppressed by combined influences from melting sea-ice, glaciers, and ice shelves, as indicated by the fast salinity drop of -5.07 ΔS per decade. This large freshening coincides with summers of minimum (~10 km^3) sea-ice export. From December 2011 to 2015 the dominance of sea-ice production with summer sea-ice exports greater than 30 km^3 is indicated by a significant salinity increase of 2.16 ΔS per decade. At this rate, assuming a threshold salinity of 34.52, SW production may be reestablished within the Sabrina Polynya by 2017.

Interannual variability of the ThW salinity is investigated in relation to the variability of zonal wind energy in the Sabrina Basin. A local index computed as the filtered (3-year window) difference of the mean surface pressure difference between the 60°S–62°S and 68°S–70°S bands (**Figure 13b**) is used as a proxy for zonal wind stress variability. It clearly indicates that minimum summer sea-ice export during July 2008 – November 2011 (**Figure 13c**) coincided with the region's minimum turbulent energy availability to breakup and export sea-ice.

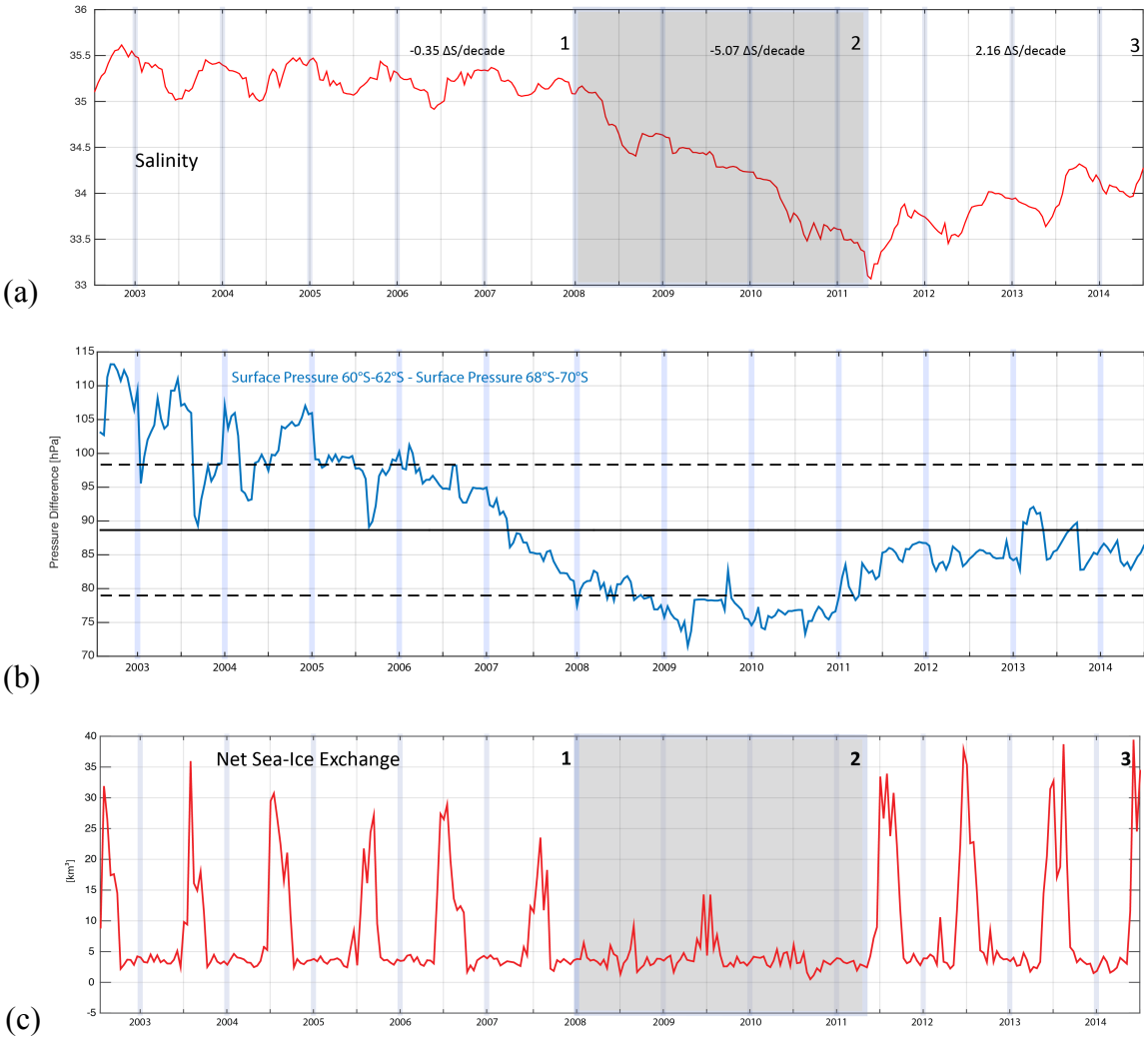

Figure 13. Time series of (a) the Thermostad Water layer salinity, (b) meridional pressure gradient with mean (solid) and one standard deviations (dashed), and (c) net sea-ice volume exchange; vertical gridlines indicate the months of January (gray) and July (blue).

8. CONCLUSIONS

A cyclonic wind pattern drives the regional oceanic circulation off the Sabrina Coast. However, the complex bathymetry found over the continental shelf, in particular along the rugged escarpment extending in front of TG-MUIS, effectively steers subsurface currents and controls the exchange across the shelf break and ice front. Thus, the interior drift of seasonal sea-ice formed within the Dalton Polynya is mainly divergent, and it supplies large volumes to the outer shelf.

Offshore transport of sea-ice across the western shelf break accounts for almost the entire (>92%) sea-ice production rate of 197.41 km^3/yr in the Sabrina Basin. During 2003-2015 sea-ice export was facilitated by the combined regional intensification (19%) of northward winds, northward sea-ice drift (24%), and sea-ice divergence (10%). Sea-ice thinned at a rate of 26.7 cm per decade, even though air temperatures exhibited small variability and sea-ice concentrations increased by only 1.6 % per decade between 2003 and 2015.

Sea-ice productivity estimated for the Sabrina Basin (4.59 m/yr) is more than twice as large as in the Adélie Basin (1.86 m/yr), and similar to the Ross Sea productivity (4.50 m/yr). Brine release during sea-ice formation in the Adélie and Ross polynyas results in dense SW production and sinking to the bottom layer of the shelf. In contrast, summer measurements show no evidence of SW in the interior of the Sabrina

Basin, even though a 150-m thick subsurface ThW layer with near-freezing temperatures (θ = -1.8°C) clearly indicates active sea-ice formation within the Dalton Polynya.

The 2003-2015 evolution of the interior ThW salinity is reconstructed based on estimated time series of local sea-ice production and the recent glacial melt rate of 90.6 Gt/yr by *Rignot and Jacobs* [2013] for the TG-MUIS system. This renders an unreasonably low (S < 31) ThW salinity and, contrary to most observations at other segments of the Antarctic shelf, a large decadal salinity increase (1.88 ΔS per decade). This study concludes that 157.5 Gt/yr of TG-MUIS glacial meltwater are required to reproduce ThW characteristics observed in the summers of 2014 and 2015, and to also result in an overall decadal freshening (-1.73 ΔS per decade) of upper waters comparable to those reported in the Ross and Amundsen seas.

Such a large local glacial freshwater input to the ThW of the Sabrina Basin layer has suppressed the effect of brine rejection from sea-ice production since 2009, thus preventing winter SW formation and convection. However, renewal of SW was indicated each winter during 2003-2008 by ThW salinities exceeding 35.25. If the estimated enhanced summer sea-ice export (>30 km^3) since 2011 continues to increase the ThW salinity at the same rate (2.16 ΔS per decade), SW formation within the Dalton Polynya could resume as soon as in 2017. Therefore, the Sabrina Basin is about to start playing an active role in the global Meridional Overturning Circulation.

REFERENCES

Comiso, J. C., R. Kwok, S. Martin, and A. L. Gordon (2011), Variability and trends in sea ice extent and ice production in the Ross Sea, *Journal of Geophysical Research-Oceans*, *116*, 1-19.

Deacon, G. E. R. (1937), The hydrology of the Southern Ocean, *Discovery Report*, *15*, 3-122.

DeLiberty, T. L., C. A. Geiger, and M. D. Lemcke (2004), Quantifying sea ice in the Southern Ocean using ArcGIS, in: *Proceedings of the ESRI International User Conference*, San Diego, CA, August 9-13, 2004, 1-14.

Gill, A. E. (1973), Circulation and bottom water production in the Weddell Sea, *Deep-Sea Research*, *20*(2), 111-140.

Gordon, A. L., P. Tchernia (1972), Waters of the Continental Margin off Adélie Coast Antarctica, in *Antarctic Oceanology II: The Australian-New Zealand sector*, edited by D. W. Hayes, pp. 59-69, American Geophysical Union, Washington, D.C.

Jacobs, S. S., C. F. Giulivi, and P. A. Mele (2002), Freshening of the Ross Sea during the late 20th century, *Science*, *297*(5580), 386-389.

Jacobs, S. S. (2006), Observations of change in the Southern Ocean, *Philosophical Transactions of the Royal Society*, *364*(1844), 1657-1681

Kusahara, K., H. Hasumi, and G. D. Williams (2011), Impact of the Mertz Glacier Tongue calving on dense water formation and export, *Nature-Communications*, *2*(159), 1-6.

Kwok, R., D. A. Rothrock (1999), Variability of Fram Strait ice flux and North Atlantic Oscillation, *Journal of Geophysical Research*, *104*, 5177-5189.

Kwok, R. (2005), Ross Sea Ice Motion, Area Flux, and Deformation, *Journal of Climate*, *18*, 3759-3776.

Massom, R. A., P. T. Harris, K. Michael, and M. J. Potter (1998), The distribution and formative processes of latent-heat polynyas in East Antarctica, *Annals of Glaciology*, *27*, 420-426(7).

Morgan, B. P. (2011), Analysis of Antarctic Sea Ice Thickness: A Newly Created Database for 2000-2009, Masters Thesis, Texas A&M University.

Orsi, A. H., T. Whitworth III, W. D. Nowlin Jr. (1995), On the meridional extent and fronts of the Antarctic Circumpolar Current, *Deep-Sea Research Part I*, *42*(5), 641-673.

Orsi, A. H., G. C. Johnson, J. L. Bullister (1999), Circulation, mixing, and production of Antarctic Bottom Water, *Progress in Oceanography*, *43*(1), 55-109.

Rignot, E., S. Jacobs, J. Mouginot, and B. Scheuchl (2013), Ice-Shelf Melting Around Antarctica, *Science*, *341*(6143), 266-270.

Rintoul, S. R. (1998), On the Origin and Influence of Adélie Land Bottom Water, in *Ocean, Ice and Atmosphere: Interactions at the Antarctic Continental Margin*, edited by S. S. Jacobs and R. F. Weiss, pp. 151-171, American Geophysical Union, Washington, D.C.

Skogseth, R., P. M. Haugan, and J. Haarpaintner (2004), Ice and brine production in Storfjorden from four winters of satellite and in situ observations and modeling, *Journal of Geophysical Research-Oceans*, *109*, 1-15.

Spreen, G., L. Kaleschlee, and G. Heygster (2008), Sea ice remote sensing using AMSR-E 89 GHz channels, *Journal of Geophysical Research, 113*.

Tamura, T., G. D. Williams, A. D. Fraser, and K. I. Ohshima (2012), Potential regime shift in decreased sea ice production after the Mertz Glacier calving, *Nature-Communications*, *3*(826), 1-6.

Tschudi, M., C. Fowler, J. Maslanik, J. S. Steward, and W. Meier (2016), Polar Pathfinder Daily 25 km EASE-Grid Sea Ice Motion Vectors. Version 3. Boulder, Colorado USA: National Snow and Ice Data Center.

van Wijk, E. M., and S. R. Rintoul (2014), Freshening drives contraction of Antarctic Bottom Water in the Australian Antarctic Basin, *Geophysical Research Letters*, *41*, 1657-1664.

Whitworth, T., A. H. Orsi, S.-J. Kim, and W. D. Nowlin (1998), Water masses and mixing near the Antarctic Slope Front, in *Ocean, Ice, and Atmosphere: Interactions at the Antarctic Continental Margin*, edited by S. S. Jacobs and R. F. Weiss, pp. 1-27, American Geophysical Union, Washington, D.C.

Wiederwohl, C. (2012), The Ross Sea Response to Evolving Ocean-Ice Interactions in a Changing Climate, Doctoral Dissertation, Texas A&M University.